Proof of Concept of QCSP Frames in Earth-to-LEO Satellite Transmission

Leonardo Montoya Obeso*, Samya Tannir*, Christian Roland*, Emmanuel Boutillon*,
Hervé Boeglen†, Rémi Chauvat‡, Vincent Deslandes‡, Matthieu Gautier§, Mickaël Friboulet*,
Jean-Michel Friedt‖, Robin Gerzaguet§, Jean-Marie Gorce¶, Raphaël Le Bidan**,
Thierry Le Gall**, Cedric Marchand*, Cyrille Morin¶, Joachim Tobias Tapparel††
*Lab-STICC, UMR 6285, Univ. Bretagne Sud, Lorient, France. †Univ. Poitiers, CNRS, XLIM, UMR 7252, Poitiers, France.
‡, Kinéis, 31520 Ramonville Saint-Agne, France. §, Univ Rennes, CNRS, IRISA, Lannion, France.
¶, Inria, INSA Lyon, CITI, UR3720, 69621 Villeurbanne, France. ‖, FEMTO-ST Temps-Fréquence, Besançon, France.
**, Lab-STICC UMR CNRS 6285, IMT Atlantique, Brest, France.
††, Institute of EE, Ecole Polytechnique Federale de Lausanne (EPFL), 1015 Lausanne, Switzerland.

***Abstract*—In this paper, we report on a multi-site experiment involving the transmission of a new type of frame for IoT, called Quasi-Cyclic Short Packet (QCSP). QCSP frames are characterized by the combination of a q-ary modulation using Cyclic Code Shift Keying (CCSK) and a q-ary non-binary Error Correction Code (ECC). A QCSP frame does not contain a preamble, making it energy-optimal since no resources are wasted for signaling. However, this absence poses a significant challenge for detection and synchronization, particularly in the case of a LEO satellite, which is subject to strong and fast-varying Doppler shifts. Our experiment demonstrates that such transmission can be successfully recovered.**

***Index Terms*—QCSP frame, Massive IoT, LEO satellite, Spatial communication, USRP.**

I. Introduction

The challenge of efficient channel access in scenarios involving the sporadic transmission of short packets by a vast number of users has gained renewed interest in the context of machine-type communication (MTC). Recent advancements have been made in waveform design, contention resolution, and coding to address this issue. While modulation and channel coding for mobile broadband applications—where a small number of users require high throughput—are well-developed and approach capacity limits, these solutions are generally unsuitable for massive IoT scenarios. This is because traditional techniques rely on closed-loop mechanisms to mitigate interference through spectral resource allocation and to estimate and compensate for channel and hardware impairments. However, in machine-to-machine (M2M) communications, maintaining continuous connectivity for millions of devices is impractical due to the excessive signaling overhead [1], [2].

Without centralized coordination, each transmitted frame must include sufficient reference signals to enable reliable activity detection and parameter estimation (such as time of arrival and the high Doppler frequency shifts experienced in low-earth orbit (LEO) satellite systems [3]). For large packet payloads, this signaling overhead is negligible compared to the total data transmitted. However, in low-payload applications like sensor networks, minimizing overhead is critical. From a physical layer (PHY) and medium access control (MAC) perspective, there is a substantial difference between 100 users transmitting 1 Mbit each and 1 million users transmitting only 100 bits each.

Historically, random access protocols based on ALOHA [4] have been used, though they suffer from significant spectral efficiency losses due to packet collisions among uncoordinated users. These protocols remain widely used in MTC over LEO satellites, where dynamic link conditions (e.g., high Doppler rates and limited satellite visibility) complicate resource allocation. They also form the basis of terrestrial Internet of Things (IoT) networks such as Sigfox and LoRa. A growing body of research now questions the suitability of grant-based random access for massive MTC [5], [6].

To improve throughput, traditional ALOHA-based protocols have evolved with contention resolution techniques such as successive interference cancellation (SIC), including contention resolution diversity slotted ALOHA [7], enhanced spread spectrum ALOHA [8], and coded slotted ALOHA [9].

In the information-theoretic domain, the concept of *unsourced* random access [10] has been introduced for scenarios where only a small fraction of nodes are active at any given time. This paradigm significantly reduces receiver complexity, allowing it to scale with the number of *active* users rather than the total number of users in the system—making it a more efficient solution for massive MTC.

In the framework of the QCSP project [11], a new type of frame called Quasi-Cyclic Short Packet (QCSP) has been proposed for the mobile channel. The use of QCSP frames has been extended to LEO satellite communication within a project led by Kinéis (a french satellite communications operator). This paper reports on a successful experiment that validates the use of QCSP frames for LEO communication. The analysis was conducted as part of the WARM-M2M project [12].

The remainder of the paper is organized into five sections. Section II introduces the QCSP frames, Section III describes the experimental setup, and Sections IV and V present the experimental protocol and the analysis of the results, respectively. Finally, Section VI provides the conclusion.

II. Description of QCSP frames

Unlike conventional telecommunication frame models that rely on a preamble for detection and synchronization, Quasi-Cyclic Short Packet (QCSP) frames are a novel frame structure that integrate directly these functions into the encoded data.

A. Structure of a QCSP frame

The structure of a QCSP frame is characterized by several elements: 1) the non-binary (NB) code for error correction, 2) the cyclic code shift keying (CCSK) modulation (inner code), 3) the symbol overmodulation and finally, 4) the BPSK chip modulation.

1) Non-Binary encoder: We consider a non-binary code defined over the Galois field with q elements, denoted by GF(q). Each GF symbol can be coded by $p = \log_2(q)$ bits, and thus can be represented by an integer between $[0, 2^p - 1]$. The input to the NB code is a binary message $\boldsymbol{U}$ of size $m = K \times p$ information bits, or equivalently, K GF(q) symbols. The NB encoder generates a codeword $\boldsymbol{C}$ of N GF(q) symbols using $\boldsymbol{C} = \boldsymbol{G}\boldsymbol{U}$, where $\boldsymbol{G}$ is the generator matrix of the code, i.e. a (N, K) matrix of GF(q). The codeword $\boldsymbol{C}$ is written as

$$\boldsymbol{C} = [c_0, c_1, \ldots, c_{N-1}]^T, \text{ with } c_k \in \text{GF}(q). \tag{1}$$

In the following, we assume that the non-binary code is a Low-Density Parity-Check (NB-LDPC) code defined by its parity-check matrix $\boldsymbol{H}$. The matrix $\boldsymbol{H}$ is assumed to be bi-regular, where each of the $N - K$ rows corresponds to a parity check of degree d_c, and each column of degree $d_v = 2$ corresponds to a variable (i.e., a GF symbol) of the code. A non-zero coefficient of $\boldsymbol{H}$ in the i^{th} row and j^{th} column is denoted by $h_{i,j}$, with $h_{i,j} \in$ GF(q). The code rate is given by $R_c = K/N = 1 - d_v/d_c$. A codeword $\boldsymbol{C}$ satisfies $\boldsymbol{H}\boldsymbol{C} = \boldsymbol{0}$, where $\boldsymbol{0}$ is the $(N - K) \times 1$ null vector over GF(q).

2) CCSK modulation: The CCSK modulation uses a pseudo-random binary sequence $\boldsymbol{P}_0 = \{P_0(i)\}_{i=0,\ldots,q-1}$ of length q with good auto-correlation properties, where $P_0(i) \in \{-1, 1\}$. The circular auto-correlation function $\theta(j)$ of a sequence $\boldsymbol{P}_0$ is defined as

$$\theta(j) = \sum_{i=0}^{q-1} P_0(i) P_0(i+j \bmod q), \quad \forall j = 0, 1, \ldots, q-1. \tag{2}$$

An ideal circular auto-correlation function satisfies $\theta(0) = q$ and should ideally verify $\theta(j) = 0$ for all $j = 1, 2, \ldots, q - 1$. In practice, for a size q equal to a power of 2, no ideal solution exists. Therefore, the quality of a sequence $\boldsymbol{P_0}$ is evaluated based on how closely its partial auto-correlation vector $(\theta(1), \theta(2), \ldots, \theta(q-1))$ approximates the zero vector. The distance is measured using the ℓ_2-norm, defined as $\ell_2(\theta) = \sum_{j=1}^{q-1} \theta(j)^2$.

A genetic algorithm was employed to construct a sequence $\boldsymbol{P}_0$ of length 64 with a minimized ℓ_2-norm. The algorithm used, along with the obtained sequences, is available online [13].

The CCSK modulation maps an element c_k of the codeword $\boldsymbol{C}$ to the sequence $\boldsymbol{P}_{c_k}$, defined as the circular right shift of $\boldsymbol{P}_0$ by c_k positions

$$\boldsymbol{P}_{c_k} = \{P_0(i - c_k \bmod q)\}_{i=0,1,\ldots,q-1}. \tag{3}$$

Hence, the CCSK frame $\boldsymbol{F}$ is defined as the concatenation of N CCSK symbols

$$\boldsymbol{F} = [\boldsymbol{P}_{c_0}, \boldsymbol{P}_{c_1}, \ldots, \boldsymbol{P}_{c_{N-1}}]. \tag{4}$$

The CCSK modulation rate can be defined as $R_m = \frac{p}{q}$, and the overall effective coding rate R_e is given by $R_e = R_c \times R_m = \frac{K}{N} \times \frac{p}{q}$. Since BPSK modulation is used, the effective spectral efficiency S_e is R_e bits per channel use.

3) Overmodulation: To facilitate the time synchronization process [14], an additional modulation, referred to as over-modulation, is applied at the symbol level to generate a known pattern of phase shifts. As a result, the QCSP frame $\boldsymbol{F}$ is defined as $\boldsymbol{F} = \{b_n \boldsymbol{P}_{c_n}\}_{n=0,1,\ldots,N-1}$, where the over-modulation is performed using the sequence $\boldsymbol{B} = \{b_n\}_{n=0,1,\ldots,N-1} \in \{-1, 1\}^N$. Similar to the sequence $\boldsymbol{P}_0$, the sequence $\boldsymbol{B}$ is designed to exhibit good auto-correlation properties.

4) BPSK modulation: Before transmission, the generated frame $\boldsymbol{F}$ consists of $n = N \times q$ BPSK symbols. It is first upsampled by a factor of $O = 30$ and then shaped by a half-raised cosine filter, h as $\{h_k\}_{k=0,1,\ldots,l_h-1}$, with a roll-off factor $\rho = 0.35$ to generate the baseband samples of the frame $F(k)$, where $k = 0, 1, \ldots, N_F - 1$, with $N_F = qNO + l_h - 1$, and l_h representing the length of the filter h.

5) Table of QCSP parameters: To conclude, generating the proposed coded frame at the transmitter side involves only simple operations (the GF encoder requires only XOR operations), making it particularly suitable for very low-cost IoT sensors. Table I summarizes all the parameters that characterize a QCSP frame.

TABLE I: Parameters of the QCSP frame used in the experiment

Symbol	Value	Comments
k	198	Payload size (in bits)
q	64	Galois Field size
p	6	Number of bits per GF symbol $(p = \log_2 q)$
K	33	Number of information symbols $(K = k/p)$
N	99	Size of outer-code codewords (in symbols)
R_c	1/3	Outer NB-code rate
P_0	$\{-1, 1\}^q$	Spreading sequence $(q = 64)$
B	$\{-1, 1\}^N$	Over-modulation sequence $(N = 99)$
R_e	0.0312	Effective coding rate $(R_e = R_c p/q)$
ρ	0.35	Roll-off factor of the HRC filter
C	6.667 kHz	Chip rate (chips per second)
S	∼9 kHz	Frame bandwidth $(C(1 + \rho))$
O	30	Oversample rate (samples per chip)
T	200 kHz	Final output rate
D	0.95 s	Frame duration $(D = Nq/C)$

III. Experimental set up

We carried out the communications experiment in collaboration with Kinéis and captured QCSP transmission from Loft Orbital's Yam-5 satellite.

A. Configuration of Earth emitter

We conducted six experimental runs, testing various configurations of QCSP frames. Across the French cities of Besançon (one, with code sign BES1), Brest (BRE1), Lannion

Fig. 1: Photo of the LAU1 and LAU2 emitters during transmission (Lausanne)

(LAN1, LAN2), Lorient (LOR1→LOR4), Lyon (LYO1, LYO2), and Poitiers (POI1), as well as Lausanne (LAU1→LAU4) in Switzerland, a total of 12 USRPs were made available for the experiment.

In this paper, we focus on a single run to illustrate the results. For this experiment, our goal was to maximize environmental diversity in a highly congested setting. To achieve this, we utilized a flyby of the YAM-5 satellite over eastern France (see Figure 5), during which the satellite recorded interfering signals spanning across Europe. Additionally, we implemented a frequency resource allocation strategy to prevent self-collisions between QCSP frames. Table II shows the central UHF frequencies allocated to each USRP device.

TABLE II: Frequency allocation of each device and the hardware used, f_0 is the central UHF frequency around 400 MHz and $\Delta f = 6$ kHz.

CS	F_0 **[MHz]**	**RF-board**	**Antenna**	**Comments**
LYO1	$f_0 - 6\Delta f$	B210	$\lambda/4$	Open field
LAU1	$f_0 - 5\Delta f$			Rooftop
LAN1	$f_0 - 4\Delta f$	X310		
LOR1	$f_0 - 3\Delta f$	SBX40	$\lambda/4$	Rooftop
LYO2	$f_0 - 2\Delta f$	B210	$\lambda/4$	Open field
LOR2	$f_0 - \Delta f$	—	—	Not used
LAU2	f_0			Rooftop
LOR3	$f_0 + \Delta f$	SBX120	$3\lambda/4$	Rooftop
LAN2	$f_0 + 2\Delta f$	X310	$\lambda/4$	
LAU3	$f_0 + 3\Delta f$		$\lambda/4$	Rooftop
LOR4	$f_0 + 4\Delta f$	SBX120	$\lambda/4$	Rooftop
POI1	$f_0 + 5\Delta f$	UBX160	$\lambda/4$	Amplifier + rooftop
LAU4	$f_0 + 6\Delta f$			Rooftop

Figure 1 displays, for example, two of the USRP boards on the roof top of an EPFL building during the experimentation.

Each frame contains a 198-bit message, consisting of 24 ASCII characters (8 bits each), followed by 6 padding bits (zero bits) to maintain the total length of 198 bits. The message format is: CS **n°** I_d**, att** A**, Freq** D", where: CS (Call Sign) is

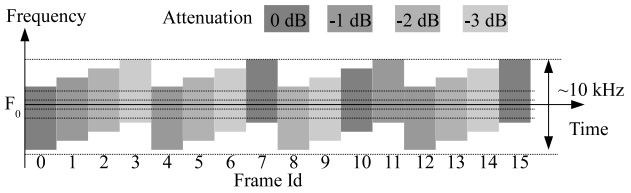

Fig. 2: Time-frequency pattern for one transmitter.

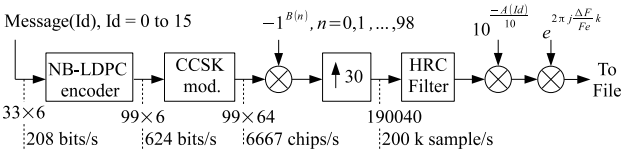

Fig. 3: Generation process of a configuration file for an USRP board.

a 4-character string identifying the emitter (see Table II). The symbol I_d is the periodic frame identifier, a number ranging from 0 to 15. The value of A determines the attenuation, in dB, of the transmitted frame. It is encoded with a single digit ($A \in \{0, 1, 2, 3\}$, the corresponding attenuation is of $-A$ dB) and the frequency offset D (also encoded as a single digit: $D \in \{0, 1, 2, 3\}$) relative to the central frequency listed in Table II. The value of A and D are computed as $A = (I_d + (I_d \div 4)) \mod 4$, where $I_d \div 4$ denotes the Euclidean division of I_d by 4. The frequency offset Δ_F is defined as: $\Delta_F = -1.5 + D$ (in kHz), with $D = I_d \mod 4$. These expressions were chosen to create an irregular emission pattern, as illustrated in the time-frequency domain in Fig. 2.

It is important to note that the emitters are not precisely synchronized. Instead, they receive a general instruction to begin transmission one minute before the satellite appears on the horizon and to stop one minute after it disappears. The transmission process involves the repeated emission of 16 frames, following the encoding scheme illustrated in Fig. 3.

The configuration of each USRP board (shown here for code sign LOR4) is provided in Fig. 4. The amplification factor is set to its maximum, corresponding to an emission power of 100 mW (+20 dBm).

B. Configuration set-up of YAM-5 satellite

The experiment took place on April 26, 2024 between 09:30 and 09:38 UTC. The trajectory of the YAM-5 satellite is shown in Figure 5.

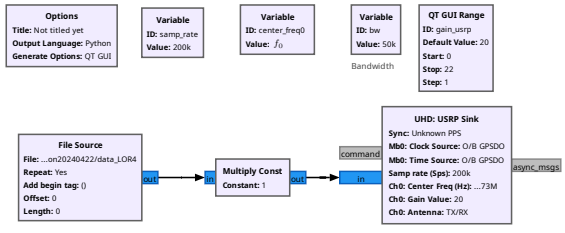

Fig. 4: GNU Radio flowchart for the generation of code sign emitter LOR4.

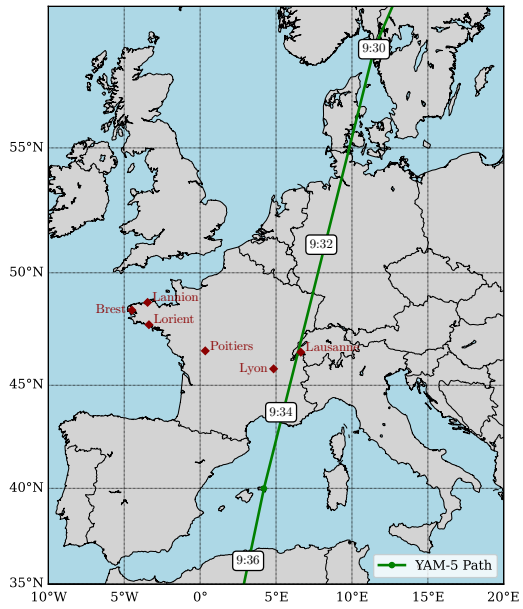

Fig. 5: Trajectory of Yam-5 satellite during the experimental setup.

TABLE III: YAM-5 satellite relative position to the city of LORIENT during experimentation.

	Pass beginning	**Max elevation**	**Pass ending**
Date	26-Apr 09:27:40	26-Apr 09:33:10	26-Apr 09:38:30
Az	21.93° (NNE)	94.82° (E)	169.49° (S)
El. (alt.)	0.41°	30.60°	1.24°
Dis. to sat.	2597.7 km	933.5 km	2485.3 km

C. Impact of the channel

The effect of the LEO channel is well documented in the literature. One model encompasses, for a given emitter c:

- An attenuation factor $\alpha(c)$ built from the received carrier power which depends mainly on the transmit power, free-space path loss, channel fade coefficient, TX/RX antenna diagrams, polarization losses and RX noise figure.
- An unknown initial phase offset $\phi(c)$.
- A frequency offset Δf_c equals to the difference between the emission frequency $f_e(c)$ and the central frequency f_0 of the receiver.
- A variable Doppler effect $f_d(c)$ that, in the experiment, could give a frequency offset varying from up to -10 kHz (when the satellite fades below the horizon) to +10 kHz (when the satellite appears on the horizon).
- A chirp effect, $a(c)$ i.e., a variation of the Doppler frequency offset between the start of the transmission and the end of the transmission. This chirp effect can have a magnitude as high as 100 Hz/s when the satellite is just at the zenith.

The received baseband signal is thus modeled as:

$$y(k) = \sum_c \alpha(c)x(k)e^{j\left[\phi(c)+2\pi k\left(\frac{\Delta f(c)+f_d(c)}{F_e}+\frac{a(c)}{2F_e^2}k\right)\right]} + w(k), \tag{5}$$

The sampling frequency is $F_e = 120kHz$. The receiver pass-band is $[f_0 - 50\text{kHz}, f_0 + 50\text{kHz}]$. This receiver configuration guarantees that all transmitted frames, even when affected by strong Doppler frequency offset, can be correctly received. Finally, $w(k)$ represents the contribution of the noise and all others interfering signals not related to the experimentation. The sampled in-phase and in-quadrature values have been stored onboard and sent back to Earth for an offline processing.

IV. Offline processing of the signal

The baseband processing of a QCSP frame has been described for the theoretical part in [14] and for the real time implementation in [15]. However, in the context of the LEO satellite, the channel is different, and some adaptations have been done to allow the detection, the synchronization and the decoding of the received frames. This section describes briefly the algorithms modifications applied to adapt the existing demodulation algorithm to the experimental conditions. The first stage of the processing is to change the sampling frequency from 120 kHz to 100 kHz in order to have exactly 15 samples per chip. The following sections describe very briefly the adaptation of [15] to a large band signal and the adaptation of [14] to take care of the frequency chirp.

A. Detection algorithm

To handle signal reception within a 100 kHz bandwidth, the receiver employs a polyphase filter bank, with Half-Raised-Cosine prototype filter, of size 2048. This approach divides the 100 kHz bandwidth into 2048 disjoint sub-bands, each with a bandwidth of 49.3 Hz. Such a narrow bandwidth allows coherent demodulation of the CCSK symbols. In fact, the maximum frequency offset within the correct sub-band is limited to 49.3/2 = 24.65 Hz, corresponding to less than a quarter of a phase rotation during the duration of a CCSK symbol.

To further reduce complexity, a downsampling by a factor of 5 is applied, decreasing the number of samples per chip from 15 to 3, which still satisfies the Nyquist criterion. In practice, the downsampling and polyphase filtering processes are performed jointly. Subsequently, the detection method proposed in [15] is applied to each sub-band. From the 2D grid score grid (time $\times$ frequency) generated, each local dominant maximum greater than a threshold gives a detection alert in a given time and frequency position. From the neighboring score values, a 2D non-coherent interpolation is performed to refine the time of arrival and frequency estimation. This step is followed by the synchronization process.

The overall complexity of the detection algorithm can be estimated by the number of multiplications and additions per second. Every second, 20000 size-2048 Fast Fourier Transforms are performed, resulting in a complexity of $20000 \times 2048/2 \times \log_2(2048) = 0.225 \times 10^9$ butterflies per second (with a butterfly operation requiring at most 6 real additions and 4 real

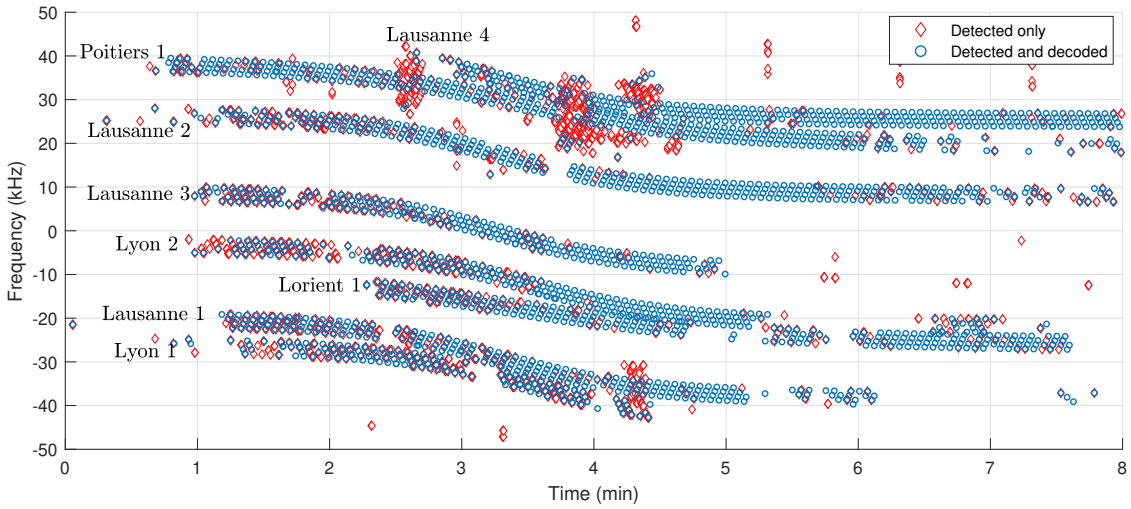

Fig. 6: Illustration in time (x-axis) and frequency (y-axis) of the received frames.

multiplications). Using the time sliding window method [15], 128 complex additions are required per time step and frequency bin, leading to a total of $20000 \times 2048 \times 128 \times 2 = 10.5 \times 10^9$ real additions per second. Assuming an 180 MHz FPGA, a minimum of 6 multipliers and 70 adders are required to support real-time processing, which is well within the capacity of modern space-grade FPGAs.

B. Synchronization

The synchronization process described in [14], [16] is not applicable directly due to the impact of the frequency chirp. To mitigate this effect, several hypotheses of chirp values are tested a priori and the one giving the best synchronization score is taken (coarse synchronization). Note that this synchronization process can declare a synchronization failure. In case of coarse synchronization success, the fine estimation process starts. The fine synchronization is performed in two steps. The frame of length 99 CCSK symbols is first split in 11 time slots, each of size 9 symbols. During the duration of a slot, the residual frequency and chirp offset are considered low enough to be neglected. Thus, a coherent summation of the 9 decoded symbols over each slot is performed, and their phase are extracted. From the size-11 vector of phases vector thus obtained, a finer estimation of residual frequency and chirp offset is performed. This process is re-iterated once considering this time 3 slots of size 33-symbols. Finally, the phase of the signal is estimated.

C. Decoding

For each detection giving rise to a synchronization success, the QCSP frame is coherently demodulated with the estimated value of phase, frequency and chirp given by the synchronization process. Then, the $q = 64$ log likelihood ratio (LLR) of each CCSK symbol are computed and sent to the non-binary LDPC decoder. The parity check matrix of the (33,99) GF(64) LDPC code is given is [17] and the decoding algorithm (extended min-sum) is available in github [18].

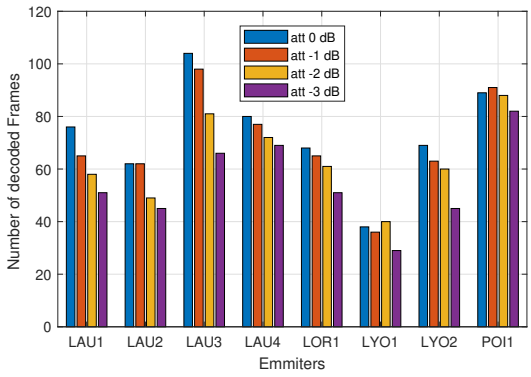

Fig. 7: Relation between number of frames per transmitter and transmitter attenuation level.

V. Result Analysis

For the proof of concept of QCSP frames in an Earth-LEO satellite communication system, no Successive Interference Cancellation (SIC) was enabled, in order to study how QCSP frames perform in this context. Figure 6 illustrates the detection (red or green points) and the corrected received frame (green points). Figure 7 gives the number of frames received as a function of the attenuation at the transmitting side for each emitter.

From these two figures, several key insights can be drawn from the experiment. Most importantly, QCSP frames can be successfully transmitted to a LEO satellite with an emission power of +20 dBm and a throughput of 208 bits/s. This result is achieved without using any preamble for frame detection and synchronization. In fact, the entire frame itself serves as a preamble for both detection and synchronization tasks. This shows that the preamble-less approach, theoretically proposed in [2], is indeed feasible in practice. However, the experiment also raises some questions. For example, although the four emitters from Lausanne were identical and co-located, there are

significant discrepancies in the number of correctly received frames (see fig. 7). Finally, among the thirteen emitters, only eight were successfully received.

Note that, in a perfect Additive White Gaussian Noise (AWGN) channel, the QCSP frame used in this experiment can be received at E_s/N_0 of -14.3 dB with a frame error rate (FER) of 10^{-2}. Given the chip rate of 6.67 kHz, this corresponds to a theoretical $C/N0$ equals to 23.9 dBHz (for a spectral occupancy of $6.67(1+\rho)$ kHz).

VI. Conclusion

This experiment demonstrates that preambles are not mandatory for transmitting short packets over an unslotted channel to a LEO satellite. This result is achieved through substantial signal processing efforts; however, hardware estimations indicate that real-time implementation on modern FPGAs is feasible. While onboard energy constraints may limit the direct use of the proposed waveform in satellite payloads, the principle of "who can do more can do less" applies. Introducing even minimal prior knowledge—such as coarse synchronization via a satellite beacon or pre-chip compensation at the transmitter—along with short training sequences could significantly reduce receiver complexity, making onboard implementation more practical.

In other words, the preambleless constraint—chosen primarily for its conceptual elegance—can be relaxed by incorporating minimal overhead to simplify the overall decoding process. Finally, the full exploitation of the experimental results is still ongoing, with further analysis and feedback from the experiments expected in the future.

Acknowledgment

This work was partially supported by the French National Research Agency (ANR) under Project ANR-24-CE25-2514, WARM-M2M ((https://warm-m2m.univ-ubs.fr).

References

[1] E. Björnson and L. Sanguinetti, "Making Cell-Free Massive MIMO Competitive With MMSE Processing and Centralized Implementation," *IEEE Transactions on Wireless Communications*, vol. 19, no. 1, pp. 77–90, 2020.

[2] G. Durisi, T. Koch, and P. Popovski, "Toward massive, ultrareliable, and low-latency wireless communication with short packets," *Proceedings of the IEEE*, vol. 104, no. 9, pp. 1711–1726, 2016.

[3] 3GPP Technical Specification Group Radio Access Network, "Study on new radio (NR) to support non-terrestrial networks," 3GPP, Tech. Rep. 38.811 V15.4.0, Sep. 2020.

[4] N. Abramson, "The ALOHA system: Another alternative for computer communications," in *Proceedings of the November 17-19, 1970, Fall Joint Computer Conference*, Houston, Texas, 1970, pp. 281–285. [Online]. Available: https://doi.org/10.1145/1478462.1478502

[5] M. B. Shahab, R. Abbas, M. Shirvanimoghaddam, and S. J. Johnson, "Grant-Free Non-Orthogonal Multiple Access for IoT: A Survey," *IEEE Communications Surveys & Tutorials*, vol. 22, no. 3, pp. 1805–1838, 2020.

[6] M. Vaezi et al., "Cellular, wide-area, and non-terrestrial IoT: A survey on 5G advances and the road toward 6G," *IEEE Communications Surveys & Tutorials*, vol. 24, no. 2, pp. 1117–1174, 2022.

[7] E. Casini, R. De Gaudenzi, and O. Del Rio Herrero, "Contention resolution diversity slotted ALOHA (CRDSA): An enhanced random access schemefor satellite access packet networks," *IEEE Transactions on Wireless Communications*, vol. 6, no. 4, pp. 1408–1419, 2007.

[8] O. Del Rio Herrero and R. De Gaudenzi, "High efficiency satellite multiple access scheme for machine-to-machine communications," *IEEE Transactions on Aerospace and Electronic Systems*, vol. 48, no. 4, pp. 2961–2989, 2012.

[9] E. Paolini, G. Liva, and M. Chiani, "Coded slotted ALOHA: A graph-based method for uncoordinated multiple access," *IEEE Transactions on Information Theory*, vol. 61, no. 12, pp. 6815–6832, 2015.

[10] Y. Polyanskiy, "A perspective on massive random-access," in *2017 IEEE International Symposium on Information Theory (ISIT)*, 2017, pp. 2523–2527.

[11] Université Bretagne Sud, *QCSP - Quasi-Cyclic Short Packet Project*, https://qcsp.univ-ubs.fr/, Accessed: 2025-10-14, 2024.

[12] Université Bretagne Sud, *WARM-M2M – Wide Area Radio Modem for Machine-to-Machine Communications*, https://warm-m2m.univ-ubs.fr/, Accessed: 2025-10-14, 2024.

[13] Emmanuel Boutillon, *PN generation, QCSP project, Deliverable D2.1*, [Accessed 2025-10-13], 2020. [Online]. Available: https://qcsp.univ-ubs.fr/wp-content/uploads/2024/09/Deliverable-D2.1.pdf

[14] K. Saied, A. C. A. Ghouwayel, and E. Boutillon, "Short frame transmission at very low SNR by associating CCSK modulation with NB-Code," *IEEE Transactions on Wireless Communications*, vol. 21, no. 9, pp. 7194–7206, 2022.

[15] C. Monière, B. Le Gal, and E. Boutillon, "Real-time energy-efficient software and hardware implementations of a QCSP communication system," *Journal of Systems Architecture*, vol. 141, p. 102 933, 2023.

[16] K. Saied, A. C. A. Ghouwayel, and E. Boutillon, "Phase synchronization for non-binary coded CCSK short frames," in *2022 IEEE 95th Vehicular Technology Conference: (VTC2022-Spring)*, 2022, pp. 1–7.

[17] E. Boutillon, *QCSP project, available http://qcsp.univ-ubs.fr*, [Online; Accessed 2023-03-21], 2023. [Online]. Available: http://qcsp.univ-ubs.fr

[18] C. O. Marchand, *Nb_ldpc_public: C code for non-binary ldcp decoder*, GitHub repository, 2020. Accessed: Mar. 16, 2026. [Online]. Available: https://github.com/Lab-STICC-UBS/NB_LDPC_FB_public